Available online at www.pelagiaresearchlibrary.com

Pelagia Research Library

Advances in Applied Science Research, 2018, 9(1):32-46

ISSN : 0976-8610
CODEN (USA): AASRFC

Control Rabi Flopping Applied to Photon Echoes for Quantum Memories

Byoung S Ham*

Center for Photon Information Processing, School of Electrical Engineering and Computer Science, Gwangju Institute of Science and Technology, South Korea

ABSTRACT

Photon echo-based quantum memory protocols presented over the last decade are primarily to solve the population inversion constraint in conventional photon echoes. In addition to population inversion, other major constraints limiting quantum memory applications are the low retrieval efficiency and short storage time, in which the importance of these factors has recently increased because of the challenges of the entangled qubit scalability and quantum repeaters. Here, I present, analyze and discuss the solution model for a Controlled Double Rephasing (CDR) echo protocol to satisfy non-inversion, near-perfect retrieval efficiency, and ultra-long storage time. In the CDR echo, a coherent Rabi pulse pair plays a key role for controlling both the ensemble phase and echo propagation direction, where the followings are the major results. Firstly, a counter propagating control Rabi pulse-pair-induced backward echo is free from echo reabsorption, resulting in a near perfect retrieval efficiency. Secondly, the control Rabi pulse pair induces an optical-spin coherence conversion like in the ultraslow light-based photon storage, resulting in a storage time extension up to spin decay time. Finally, the control Rabi flopping to a third state induces a π phase shift to the ensemble coherence, resulting in an emissive echo in the double rephasing scheme, where the π phase shift is due to optical-spin coherence conversion process.

Conclusion: *This study reveals that TORCH infections require serious attention as these infections cause serious abnormalities and anomalies in children as well as to pregnant females.*

Keywords: Quantum physics, Quantum information, Optics, Strongly correlated materials

INTRODUCTION

Over the last two decades, quantum technologies have been employed toward potential applications of quantum cryptography [1-4] and quantum computers [5-7]. Although qubit scalability has recently been demonstrated for up to 51 controllable qubits [8], entangled qubit scalability has still been remained as a problem, where the main constraint is quadratically increased decoherence with respect to the entangled qubit number [9]. Especially, quantum error corrections necessary for fault-tolerant quantum computing need hundreds or thousands of redundant qubits [6], where each quantum gate operation accumulates errors mainly due to individual qubit decoherence at each stage. Thus, both ultralong coherence and near unity retrieval efficiency of qubits become essential factors for the implementation of quantum technologies. In long-distance quantum communications based on quantum repeaters [10], the transmission (entanglement swapping) distance increases logarithmically as the qubit coherence time increases. According to the quantum repeater protocol, a quantum memory as an essential hardware component needs minute-order storage time for just a ~500 km entanglement swapping distance [11]. So far, such an ultra-long quantum memory has not yet been demonstrated. Here, the quantum memory should be compatible with optical photons for access to a free space or an optical fiber. Thus, an active control of decoherence in qubits has become one of the most important tasks in quantum technologies, where the ultra-long quantum memory with near perfect retrieval efficiency paves a road to both circuit- [5,6,12] and measurement-based [12,13] quantum computing as well as long distance quantum communications based on quantum repeaters [10,11].

In light-matter interactions, light absorption strongly depends on the interaction cross section in the matter, where an ensemble has the benefit of a large cross section compared with a single atom, eliminating the use of an optical cavity [14]. In general, an ensemble whose broadening is inhomogeneous has a fundamental defect of ultrafast decoherence, preventing its use as a qubit. Photon echoes turn this defect into a benefit via a rephasing process, where rephasing is a reversible coherence evolution process activated by an optical π pulse [15]. This makes the photon echo effective in quantum information processing with both wide bandwidth and multimode functionality. This π pulse-induced reversible coherence evolution, however, results in population inversion, preventing photon echoes from quantum memory applications due to potential quantum noises by a spontaneous or stimulated emission process. Thus, modified photon echo schemes have been sought over the last decade for the use of the multimode and wide bandwidth functionality for quantum memories [16-30]. Here, the photon echo is simply a retrieved coherence burst of the initially excited coherence in the matter by a (quantum) light pulse. In modified photon echo methods such as Controlled Reversible Inhomogeneous Broadening (CRIB) [16,17], gradient echoes [18-21] and atomic frequency comb (AFC) echoes [22-26], population inversion has been removed by not using the π optical pulse [17]. However, Doppler shifts [16], spectral tailoring [18] or a long AFC preparation time [22] makes the system inefficient or impractical. To keep all benefits of photon echoes, quantum coherence control has recently been adapted for an ensemble phase control, especially for extending the photon storage time up to spin population relaxation time, T_1 [27-30].

Double Rephasing (DR) in photon echoes offers the inherent benefit of having no population inversion. However, the coherence of the second DR echo becomes absorptive and thus impractical unless the echo phase is controlled to be extracted from the optically dense medium [31-33]. Therefore, the first DR echo must be erased or silenced; otherwise it affects the second echo due to coherence retrieval of the ensemble [31]. Here, it should be noted that recently observed DR echoes [31-33] violate the relation between absorptive coherence and echo emission, where echo emission is simply due to coherence leakage by Gaussian light pulses spread out over the transverse spatial domain [34].

To solve absorptive coherence in DR echoes [31-33], quantum coherence control in a three-level system has been adapted [28-30]. In a three-level system, resonant Raman pulse excited two-photon (spin) coherence results in a π/2 phase shift with respect to the optical coherence [35]. This quarter wave relation induced by a control Rabi pulse is the origin of the ensemble phase control, which is the novelty of the present paper. Although stop-light experiments have been intensively studied for quantum memories in the 2000s [36-38], the phase shift in the coherence transfer between optical and spin states has not drawn much attention because there is no need for spin rephasing in cold atoms [36] or atomic vapors [37]. Spin inhomogeneity, however, is a critical matter for rephasing in solids, where the optical phase matching condition for stop light recovery cannot be met without it [38]. In the present paper, a new quantum memory protocol of controlled double rephasing (CDR) photon echoes is introduced, analyzed, and discussed for collective atom phase control in a solid ensemble for practical quantum information applications. For this, various modified photon echo schemes are reviewed, compared with each other, and discussed regarding the basic mechanisms, including ensemble phase control.

In Section A, both conventional photon echo and the first modified photon echo, i.e., CRIB are reviewed to elucidate the fundamental physics of coherent transients, where in CRIB the rephasing is accomplished by opposite Doppler shift-induced ensemble phase shift, resulting in no population inversion. In Section B, the origin of the ensemble phase shift by control Rabi flopping in a three-level system is analyzed and discussed, revealing the fundamental physics of coherence control in an ensemble. In Section C, the DR echo scheme is analyzed regarding ensemble phase evolutions, and its impracticality based on absorptive echoes is discussed; some related DR echo techniques are criticized as well. In Section D, one example of the dc Stark echo protocol in the modified DR echoes is analyzed and discussed in terms of the silencing mechanism of the first echo. In Section E, the CDR echo scheme is introduced, analyzed and discussed for the atom phase control, resulting in a near perfect, and ultra-long, multimode quantum memory protocol. For these, a full numerical approach is adapted to continuously trace individual atom phase evolutions in light-matter interactions. In addition to the detailed numerical calculations, intuitive analytical solutions are also sought using a simple phase evolution process obtained by the interaction Hamiltonian approach. For the atom phase control in CDR echoes, control Rabi flopping becomes the most important aspect of coherence control, satisfying both ultra-long storage and near perfect retrieval efficiency.

METHODS: NUMERICAL CALCULATIONS

For the numerical calculations presented in all figures, all decay rates are set to zero for clear visualization of individual

atom-phase evolutions. The density matrix approach is powerful in dealing with an ensemble medium for light-matter interactions, especially when continuously tracing the coherence evolutions of individual atoms. Thus, the phase evolutions can be clearly visualized for (modified) photon echoes, including CDR echoes. For the analytic approach, the simple phase term of each atom under a rotating wave approximation in the interaction Hamiltonian is used to show how each atom's phase evolves in the time domain with and without interacting optical fields. The equations of motion of the density matrix operator ρ are determined by the Liouville-von Neumann equation:

$$\frac{d\rho}{dt}=\frac{i}{\hbar}[H,\rho]-\frac{1}{2}\{\Gamma,\rho\}$$

The following equations are time-dependent coherence terms of $\dot{\rho}_{ij}$ in a lambda-type, three-level system interacting with two resonant optical fields, obtained by solving the time-dependent Schrodinger wave equations, $i\hbar|\dot{\Psi}=H|\Psi$ H is the interaction Hamiltonian $\rho=|\Psi\Psi|$) [39]:

$$\frac{d\rho_{12}}{dt}=-\frac{i}{2}\Omega_1\left(\rho_{11}-\rho_{22}\right)-\frac{i}{2}\Omega_2\rho_{13}-i\delta_1\rho_{12}-\gamma_{12}\rho_{12} \quad (1)$$

$$\frac{d\rho_{13}}{dt}=-\frac{i}{2}\Omega_2\rho_{12}+\frac{i}{2}\Omega_1\rho_{23}-i(\delta_1-\delta_2)\rho_{13}-\gamma_{13}\rho_{13} \quad (2)$$

$$\frac{d\rho_{23}}{dt}=-\frac{i}{2}\Omega_2\left(\rho_{22}-\rho_{33}\right)+\frac{i}{2}\Omega_1\rho_{21}+i\delta_2\rho_{23}-\gamma_{23}\rho_{23} \quad (3)$$

Here Ω_1 is the Rabi frequency of the resonant optical field (related to photon echoes) between the ground state $|1\rangle$ and the excited state $|2\rangle$, Ω_2 is the Rabi frequency of the resonant control field between the auxiliary ground state $|3\rangle$ and the excited state $|2\rangle$ and δ_1 (δ_2) is the atom detuning from the resonance field Ω_1 (Ω_2). Instead of using Maxwell-Bloch equations as is done in many photon echo studies with appropriate approximations, we focus on the coherence evolutions of individual atom phases in the time domain without any assumptions. Although complete light-matter interactions can be solved by combining both density matrix equations and Maxwell-Bloch equations, a complete solution has been limited to the short time scale of picoseconds in a personal computer environment, due to limited computing power [40].

For all numerical simulations, nine total time-dependent density matrix equations including equations (1)-(3) are calculated without any approximations. For this, an in homogeneously broadened lambda-type three-level optical system is chosen, where the optical inhomogeneous broadening and the interacting optical Rabi frequencies are chosen to be similar to the experimental parameters used in a rare-earth Pr^{3+} doped Y_2SiO_5 (Pr:YSO) [41]. The actual optical and spin decay rates of Pr:YSO are negligibly small down to ~kHz or less compared to the optical inhomogeneous broadening. Here, the optical inhomogeneous broadening of Pr:YSO can be experimentally manipulated via spectral hole-burning owing to the ultra-long spin relaxation decay time among three hyperfine states in the ground level. The optical inhomogeneous broadening is assumed to be Gaussian. In each figure, the optical inhomogeneous broadening is divided into a certain number (81-161) of atom groups with a 10 kHz spectral spacing, then each atom group is calculated in both the time and spectral domains with a different weight factor given by the Gaussian profile at a different detuning. Finally, all individual density matrix calculations are summed together for the overall coherence evolution in the time domain.

RESULTS AND DISCUSSION

Review of modified photon echoes for population inversion removal

Figure 1 shows the fundamental physics of the storage mechanism of conventional two-pulse photon echoes in a two-level system, where the π optical pulse R reverses all in homogeneously broadened atoms' phase evolutions triggered by the data pulse D, resulting in a photon echo. For photon echoes, the medium must be in homogeneously broadened and the data pulse spectrum must be within this broadening. Each optical pulse is assumed to be monochromatic with a rectangle pulse shape for simplicity. In Figure 1a, the initial coherence of the system is ρ_{ij}=0, except for ρ_{11}=1. Figure 1b shows the calculation result for Figure 1a, while Figure 1c is for a 3D picture of Figure 1b. Figure 1d is the

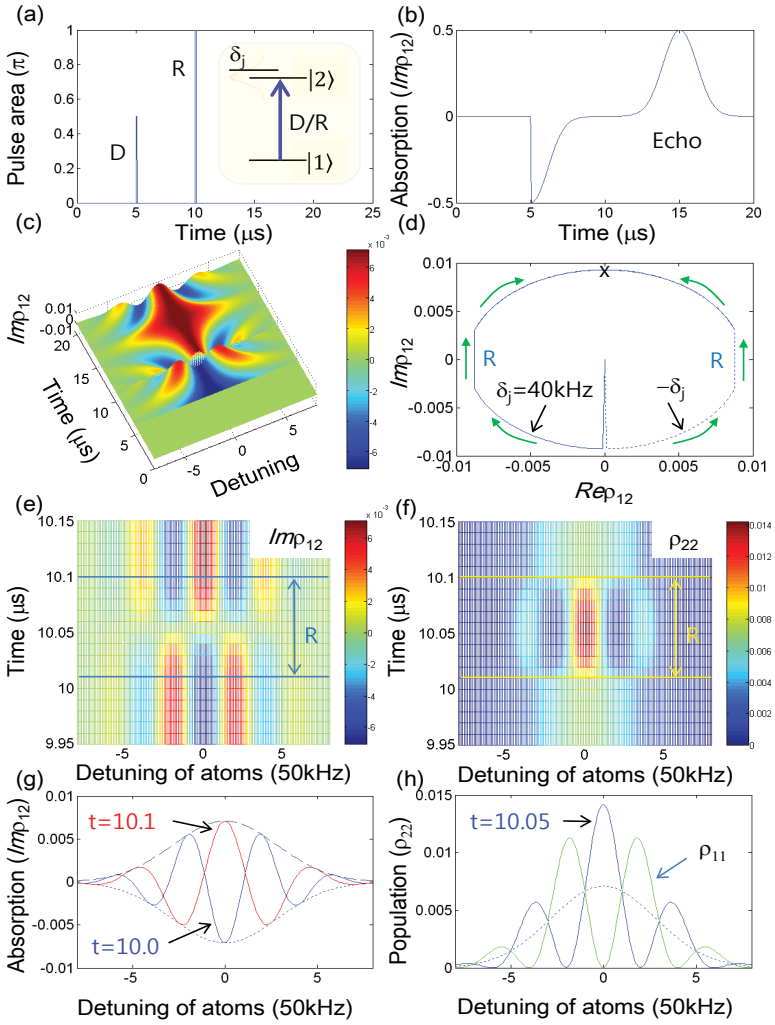

Figure 1: Storage mechanism in photon echoes. (a) A schematic of two-pulse photon echoes. The pulse arrival time for D (R) is t=5 (10) with 0.1 μs pulse duration. All decay rates are set to zero. Inset: Energy levels of inhomogeneously broadened atoms (FWHM: 340 kHz). (b) Numerical calculations for (a). The photon echo appears at t=15. (c) A 3D color map of (b) for all spectral distributions. (d) A Bloch vector diagram for a detuned atom pair at $\delta_j = \pm$ 40 KHZ. The mark 'x' is for the echo timing. (e) and (f) Details of (c) for rephasing during $10.00 < t \leq 10.10$. (g) Details of (c) for phase grating at t=5.1 (dotted, D), t=10.0 (blue, before R), t=10.1 (red, after R), and t=15.0 (dashed, echo). (h) Details of (c) for population grating (ρ_{22}) at t=5.1 (dotted, D), t=10.05 (blue, middle of R). The green curve is for ρ_{11} at t=10.05 (middle of R). In the programming the time increment is 0.01 μs, where R is turned on at t=10.01 μs during $10.00 < t \leq 10.10$. The time unit is μs. For calculations, 99.55% of the optical inhomogeneous width is divided into 81 groups with 10 kHz spectral spacing

coherence evolutions of a symmetrically detuned atom pair, where the evolution direction is determined by the atom detuning sign from the resonance frequency. The mark 'x' in Figure 1d indicates the photon echo generation position, resulting in a π phase shift. As shown in Figures 1e and 1g, in homogeneously broadened atoms excited by D (π/2 pulse area) induce a phase grating in its spectral domain of the ensemble medium, where the modulation frequency of the phase grating is time-dependent determined by $1/(t-t_\rho)$. By the π pulse of R, this phase grating gains a π phase shift due to population inversion in equation (1), resulting in rephasing (see the color change in Figure 1e).

$$\rho(t)\rho(t) \rightarrow \rho(t)^*$$

This means that the coherence evolution direction is reversed by R, and thus a photon echo generates as the retrieved coherence for the D-excited ensemble. Thus, phase grating becomes the storage mechanism in two-pulse photon echoes. For multiple data pulses, the echo sequence is obviously reversed by the rephasing mechanism.

When the rephasing pulse R is evenly divided into two (delayed) pulses whose pulse areas are π/2 each, the conventional three-pulse photon echo scheme is satisfied [42]. In Figures 1e and 1f, the phase grating at t=10.0 μs just before R is now converted into a population grating by the first half R, at t=10.05 μs. In Figures 1g and 1h (blue curves), the

modulation frequency is calculated at 200 kHz ($(t-t_D)^{-1}$) at t=10.0 μs; t-t_p5 μs. When the second half R interacts, the population grating in Figure 1f switches to the phase grating with a π phase shift (see the color swapping along R in Figure 1e). Here, the important physics is that the coherence conversion between phase and population gratings is reversible. Thus, the population grating becomes the storage mechanism in conventional three-pulse photon echoes, as proven even for quantum memories based on atomic frequency comb (AFC) echoes [22-26]. Here, AFC uses a phase matched population grating constructed and accumulated by many consecutive weak two-pulse sets as a storage medium, where the AFC grating can last up to the spin population relaxation time. Because the data retrieval process in AFC echoes is actually initiated by the READ (the second half of R) pulse in the three-pulse photon echoes, the AFC storage time is limited by the phase grating. Unlike the three-pulse echoes, consecutive quantum data storage (this is actually consecutive READ process) in AFC echoes, therefore, results in the same echo sequence, where the multiple readouts are owing to the accumulated coherence [24]. This is the correct understanding of AFC echoes, where the storage time is too short to be applied for quantum technologies (Figure 1).

In the programming the time increment is 0.01 μs, where R is turned on at t=10.01 μs during 10.00<t ≤ 10.10. The time unit is μs. For calculations, 99.55% of the optical inhomogeneous width is divided into 81 groups with 10 kHz spectral spacing.

The first trial to solve the population inversion constraint in conventional photon echoes was done in both a Doppler medium [16] and a non-Doppler medium [17], referred to as CRIB. In the CRIB echo scheme of Figures 2a and 2b, a counter-propagating control pulse set (C1 & C2) excites opposite Doppler shifts on the same moving atoms, where the opposite Doppler shifts resemble a symmetrically detuned atom pair as seen in Figure 1d. This symmetric detuning effect combined together with Rabi flopping-induced coherence conversion mimics the rephasing in photon echoes as shown in Figure 2c [27-30,35]. Thus, a photon echo without population inversion is achieved. In Figure 2f, the opposite Doppler shifts are visualized to show a different mechanism for the time reversal process in Figure 1d. The CRIB mechanism in Figure 2, however, needs to be modified when applied to a solid medium due to no Doppler effects [17]. Here, the population transfer to the third state $|3\rangle$ results in a storage-time extension up to spin T_2, where spin T_2 is similar to spin T_1 if the thermal spin bath is frozen, e.g., by applying zero first-order Zeeman field [43] or dynamic decoupling [44]. Moreover, the backward control pulse set satisfies non-degenerate phase conjugation and results in a near perfect retrieval efficiency with a backward echo even in an optically dense medium [16,45] (Figure 2).

The idea of CRIB has been adapted to gradient echoes in a two-level solid medium [18], where reversed dc electrode pairs replace the control pulses in the CRIB technique of Figure 2a, resulting in the same effect as rephasing without population inversion. For this, spectral tailoring is a prerequisite for an optically dense and spectrally narrow solid ensemble. The following opposite gradient electric fields result in rephasing by reversing the sign of detuning in each atom. Unlike conventional photon echoes governed by Beer's law, where there is a severe echo reabsorption problem, CRIB-based modified photon echoes offer very high echo retrieval efficiency [19]. In the gradient echoes, the high echo efficiency is obtained by using the reversed spatial gradient of the atom distribution so that there is no echo reabsorption along the longitudinal axis, as is the case for the backward echo in CRIB. For the storage time extension, the gradient echo is modified by adding a control pulse for the Raman scheme [46,47]. This modified gradient echo technique [20,21], however, never works in a solid ensemble due to spin inhomogeneity necessary for spin rephasing as demonstrated in both slow-light-based quantum memories [38] and resonant Raman echoes [46,47]. Moreover, the off-resonant Raman scheme never satisfies a complete population transfer between the Zeeman states, resulting in very low retrieval efficiency for multimode storage [24].

The third attempt to solve the population inversion problem in photon echoes was done by AFC echoes [22]. The AFC technique is based on population grating in a persistent spectral hole-burning medium composed of at least three energy levels. Unlike the three-pulse photon echoes whose grating is formed by consecutive two pulse pair, a repeated weak two-pulse train renders the population (grating) coherence accumulated, while removing the excited population to an auxiliary third state. Although such accumulated coherence in the ground state grating can enhance the echo efficiency based on Kerr nonlinear optics, there is always a trade-off between data absorption and echo reabsorption, resulting in limited retrieval efficiency far less than 50% [22-26]. Moreover, the AFC [48], to extend the photon storage time in AFC echoes, the same control Rabi pulse pair has been adapted in a forward scheme [25]. However, the modified AFC echo scheme with the π-π control Rabi pulses is not correct because of the Rabi flopping-induced coherence inversion as shown in Figure 2e, resulting in an absorptive echo [16,17,46-49]. Here, the control Rabi

flopping-induced coherence inversion has no relation with its propagation directions.

The fourth technique for solving the population inversion problem in photon echoes was presented by CDR echoes [29]. Because each π optical pulse in a two-level system induces a population inversion, double π pulses should fix the inversion problem of DR echoes. To work with the CDR echo protocol for quantum memories, however, the following requirements must be satisfied.

Requirement I: The first echo generated by the first π optical pulse must be killed (erased or silenced) in order to not affect the second echo.

Requirement II: The second echo must be emissive in collective atom coherence.

For the first requirement, a silent echo concept with on-demand phase mismatching between the data and the first echo has been firstly presented [31]. Because a photon echo is a direct result of a macroscopic (or collective) coherent transient effect, an easy way to destroy echo formation is simply to add phase turbulence or to violate the phase matching condition. Such a silent echo can also be obtained by using the dc Stark effect [50,51], magnetic effect-based phase turbulence [52,53] or ac Stark effect [30,54]. Although the first echo e1 is removed, however, the second echo is still absorptive in refs. [31-33,54]. Like the controlled AFC, DR echoes cannot be extracted from the medium, where the echo observations are due to coherence leakage by the Gaussian rephasing pulses [34]. The all-pervasive misunderstandings of coherence in photon echoes and the modified methods mentioned above have motivated in the present paper, and I now present the quantum coherence control for a correct solution of DR echoes that satisfy the second requirement of the CDR echo.

Analytic expression for coherence inversion via control rabi flopping

Before discussing the CDR echoes, optical Rabi flopping in a resonant Raman system needs to be analyzed with a simple state vector approach using the Schrodinger wave equations. Here, our interest is how the Rabi flopping due to the control pulse C affects the ensemble coherence excited by a data pulse D (Figure 3a). The coherence conversion process between optical and spin states has already been analyzed as a key mechanism in the modified photon echoes for quantum memories [35,47]. In Figure 3, control Rabi flopping-affected optical coherence in a resonant Raman system is analyzed and compared with the results of a two-level system. The two-level system in Figure 3a is simply obtained by setting $\Omega_C = 0$ and $\gamma_{23} = \gamma_{13} = 0$. For this, two different schemes are independently shown in Figure 3b. Figures 3c-3f shows the numerical calculations for Figure 3b. In Part I, the analytical approach is performed using state vector notations in the time-dependent Schrodinger wave equations, and then it is compared with numerical results obtained by solving density matrix equations. In Part II, the physics discussed in Part I is applied to a real system of photon echoes and discussed for the coherence control of echo signals.

Part I

Via the data pulse excitation with Rabi frequency Ω_D for the first part in Figure 3b, the state vector $|\Psi(t)_D$ resulting from atom-field interactions is described by:

$$|\Psi(t)_D = \cos\left(\frac{\Omega_D t}{2}\right)\left|1 + i\sin\left(\frac{\Omega_D t}{2}\right)\right|2 \tag{4}$$

Thus, the optical coherence $\rho_{12}\left(=c_1 c_2^*\right)$ is denoted by $-i\cos\frac{\Omega_D t}{2}\sin\frac{\Omega_D t}{2}\left(=-\frac{i}{2}\sin\Omega_D t\right)$, resulting in a Rabi oscillation with frequency Ω_D (see the first parts of Figures 3c-3f). The excited state population $\rho_{22}\left(=c_1 c_2^*\right)$ is described by $\sin^2\left(\frac{\Omega_D t}{2}\right) = \frac{1}{2}\left(1-\cos\left(\Omega_D t\right)\right)$. Therefore, the coherence oscillation frequency exactly matches the population counterpart (see also the numerical results in Figures 3c and 3d.

For a three-level Raman system of Figures 3a (second part of Figure 3b), the state vector $|\Psi(t)_R$ is described for the optical Rabi frequencies Ω_D and Ω_C:

$$|\Psi(t)_R = \left[\frac{\left(\Omega_C^2 + \Omega_D^2 cos\left(\frac{\Omega t}{2}\right)\right)}{\Omega^2}\right]\left|1 + i\frac{\Omega_D}{\Omega}\sin\left(\frac{\Omega t}{2}\right)\right|2 + \frac{\Omega_D\Omega_C}{\Omega^2}\left[\cos\left(\frac{\Omega t}{2}\right) - 1\right]|3 \tag{5}$$

Here, Ω_C is the Rabi frequency of the pulse C, and Ω is the generalized Raman Rabi frequency, where $\Omega = \sqrt{\Omega_D^2 + \Omega_c^2}$.

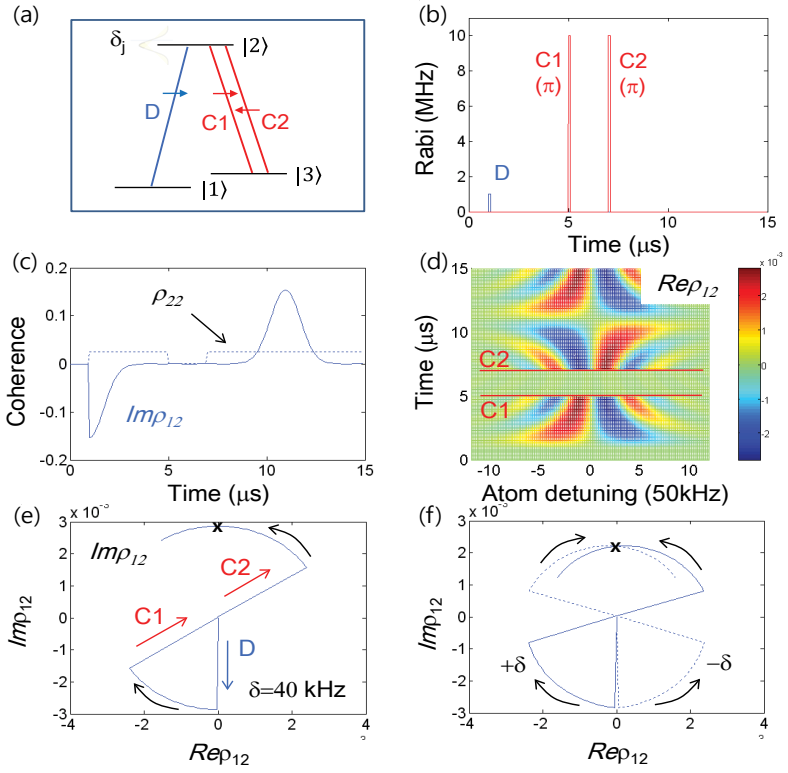

Figure 2: Controlled reversible inhomogeneous broadening (CRIB) echoes. (a) and (b) Schematics of CRIB echoes. (c) Numerical results of (b). (d) A 3D plot of (c) for $Re\rho_{12}$. (e) A Bloch vector model for a detuned atom's coherence evolution. (f) A Bloch vector model for a symmetrically detuned atom pair at $\delta = \pm 50$ kHz with $\Gamma_{21}=\Gamma_{23}=5$ kHz. The optical inhomogeneous width is 510 kHz (FWHM). For calculations, 99.55% of the optical inhomogeneous width is divided into 121 groups with 10 kHz spectral spacing. The mark 'x' in (e) and (f) denotes the echo timing. All decay rates are zero, otherwise specified

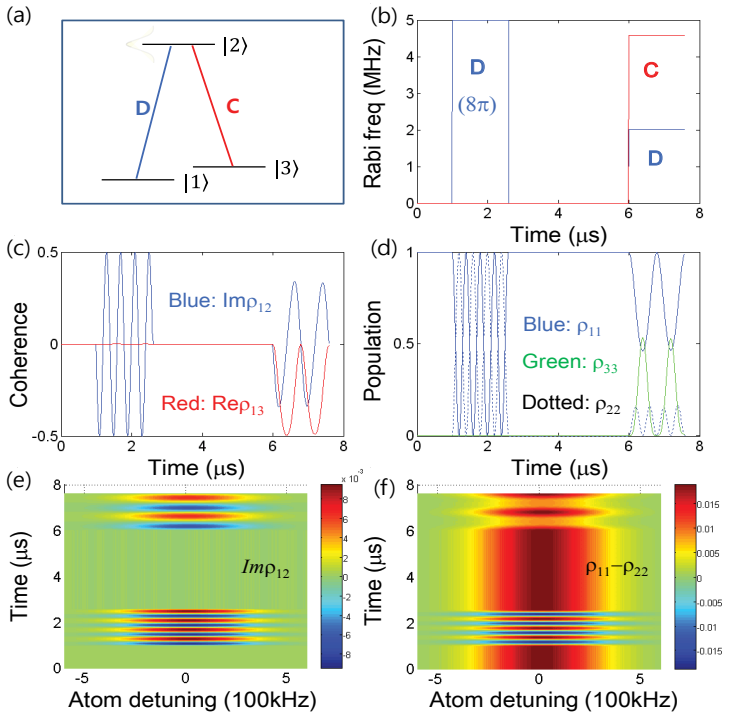

Figure 3: Direct vs. indirect coherence excitations. (a) and (b) Schematics of atom-light interactions for direct (D only) and indirect (D and C; resonant Raman) coherence excitations. The pulse area of D and Raman is 8π each. (c) and (d) Overall coherence and population oscillations for (b). A 3D color map of (e) $Im\rho_{12}$ and (f) $\rho_{11}-\rho_{22}$ for (b). The optical inhomogeneous broadening is 510 kHz (FWHM). Initially all $\rho_{ij}=0$, except for $\rho_{11}=1$. For calculations, a total 99.55% of the optical inhomogeneous width is divided into 121 groups at 10 kHz spacing

For $\Omega_C \gg \Omega_D$ satisfying the quantum memory condition, the control pulse Ω_C (~Ω) in Equation 5 becomes a dominant factor:

$$|\Psi(t)_R \cong |1+\frac{\Omega_D}{\Omega}\left[\cos\left(\frac{\Omega t}{2}\right)\middle|3+i\sin\left(\frac{\Omega t}{2}\right)\middle|2\right] \quad (6)$$

Thus, the optical coherence $\rho_{22}\left(=c_1c_2^*\right)$ in a Raman system is proportional to $-isin\frac{\Omega_D t}{2}$, which has a twice slower oscillation frequency compared with that in a two-level system (see the second parts of Figures 3c-3f). Note that the exact form of ρ_{12} can be derived from equation 5 as:

$$\rho_{12}(t) = -i\frac{\Omega_D\left[\Omega_C^2+\Omega_D^2 cos\left(\frac{\Omega t}{2}\right)\right]sin\left(\frac{\Omega t}{2}\right)}{\Omega^3} \quad (7)$$

Where, $\rho_{12}(t) = -i\frac{\Omega_D}{\Omega}sin\left(\frac{\Omega t}{2}\right)$ for $\Omega_C \gg \Omega_D$. On the other hand, the oscillation frequency of the excited state population ρ_{22} in equation 5 is the same as that in the two-level system (see also the dotted curve in Figure 3d). Thus, control Rabi flopping by C for the excited state atoms ρ_{22} induces a π phase shift in the ensemble coherence ρ_{12} in a three-level system. Such a coherence inversion has already been discussed in resonant Raman echoes [46,47]. In other words, control pulse-induced (Raman) Rabi flopping inverts the system coherence at every 2π of $\Omega T : |\Psi(t+T)_R = -|\Psi(t)_R$. This control Rabi flopping is also shown in the CRIB case of Figure 2e with Doppler effects. Here, it should be noted that the origin of the coherence inversion via control Rabi flopping belongs to the Raman coherence ρ_{13} as shown in Figure 3c [35].

Part II

What happens if the pulses D and C in the resonant Raman scheme of Figure 3b are temporally separated? Figure 4 is an extension of Figure 3 for the delayed Raman scheme, which is helpful for understanding CDR echoes. In nonlinear optics, the time delay between the resonant Raman pulses must be shorter than the inverse of the optical inhomogeneous width [55]. This is the direct result of macroscopic coherence for the phase matching condition. However, in the coherent transients such as photon (spin or Raman) echoes, this rule is no longer effective, because rephasing is involved [56] (Figure 4).

The collective (overall) Raman coherence excitation ρ_{13} in a delayed scheme of Figure 4a is zero at all times due to the delay longer than the inverse of the optical inhomogeneous width. Thus, the $\gamma^{(3)}$-dependent nonlinear effect is also nullified. The collective (overall) optical coherence ρ_{12} decays as a function of the inverse of the optical inhomogeneous broadening [1/(510,000π)=0.6 μs]: optical FID. However, individual atoms are independent of the FID, but dependent on the optical homogeneous decay time (Figure 4b). Both optical and spin homogeneous decay rates are set to zero for simplicity. The optical coherence ρ_{12} of individual atoms oscillates at a twice slower speed in the delayed Raman system (Figures 4b and 4c). Thus, a 2π control pulse C induces coherence inversion ($\rho_{12} \rightarrow -\rho_{12}$) as discussed in equations (5) and (6) (Figure 4d). This means that a 2π (4π) control pulse C applied to photon echoes results in an absorptive (emissive) echo, as shown in Figure 4e (see the dotted (solid) curve) [57]. Figure 4f represents that the single 4π pulse area of C in Figure 4e can be divided into two control pulses, C1 (π) and C2 (3π) [56,57] for the same result. The maximum delay of C2 from C1 is determined by the spin dephasing time [25,56]. There is always trade-off between the echo efficiency and storage time. In the CDR echo with the control Rabi flopping, the storage time can be extended by many orders of magnitude without nearly sacrificing the echo efficiency.

Although the 2π (or π-π) control pulse C in Figure 4g gives the same coherence inversion as in CRIB (Figure 2e), the rephased coherence evolution direction does not change in solids, resulting in an absorptive echo. This is the fundamental difference between Doppler [16] and non-Doppler [17] media in the application of control Rabi flopping. Thus, unlike the π-π control pulse sequence in a Doppler medium [16], the same control pulse sequence does not work in a solid medium [17,56,57]. In other words, the controlled AFC echo with a π-π control pulse sequence [25] in a solid medium results in an absorptive echo, where AFC is based on a single rephasing scheme of three-pulse photon echoes as discussed already [24,47-49]. The proof of principle of the phase dependent absorptive echo was demonstrated in the resonant Raman scheme [46,47]. Thus, experimental observations of the controlled AFC echoes are simply due to imperfect rephasing by Gaussian control light whose spatial distribution in the transverse mode results in many

different pulse areas [34]. These effects partially violate the atom phase recovery condition of 4nπ of the control Rabi flopping in Figure 4h. Thus, any rephasing pulse area can generate a photon echo experimentally. Only matter is reduced echo efficiency [33]. To solve the absorptive echo problem in Figure 4g (see the mark 'x') [25], another 2π control pulse is needed, as shown in Figure 4h. Full analytical expressions have also been presented [58]. With counter-propagating control pulses C1 (π) and C2 (3π), the echo direction $\boldsymbol{k}_E$ is predetermined backward with respect to $\boldsymbol{k}\rho(\boldsymbol{k}_E=-\boldsymbol{k}\rho=\boldsymbol{K}_{c1}=\boldsymbol{k}_{c2})$, satisfying near perfect retrieval efficiency η_e [16,45,59].

$\eta_e=(1-e^{-d})^2$, where d is the optical depth.

Ananytic expression for doubly rephased photon echoes: Understanding macroscopic coherence evolution

A doubly rephased two-pulse photon echo in a two-level system is analyzed in Figure 5. Initially all atoms are in the ground state $|1\rangle : \rho_{11}=1; \rho_{12}=0$. Figure 5b shows the numerical results, where the first echo e1 and the second echo e2 are opposite in terms of coherence as expected. Figure 5c shows the phase evolution of a δ_j-detuned atom. Here, the free evolution after each pulse is described by only the function of its detuning δ_j under the rotating wave approximation of the interaction Hamiltonian (unitary evolution): $\Psi(r,t)=\Psi(r)e^{\pm i\delta_j t}$. For simplicity, let tρ=0 and t_R-$t_D \equiv T$ where t_z represents the arrival time of pulse z. The detuning $\pm\delta_j$ is for a symmetrically detuned ± jth atom pair from the line center of 2N contributed atoms in an optical inhomogeneous broadening $\Delta=\sum_{-N}^{N}\rho_{jgj}$; g_j is a Gaussian weight factor. As shown in Figures 5c and 5d, the first π pulse R (c-d) rephases the individual coherence with a π phase shift at $t=t_R=T$ and individual atom phase evolutions continue to evolve in the t' time domain (see the interval d-e):

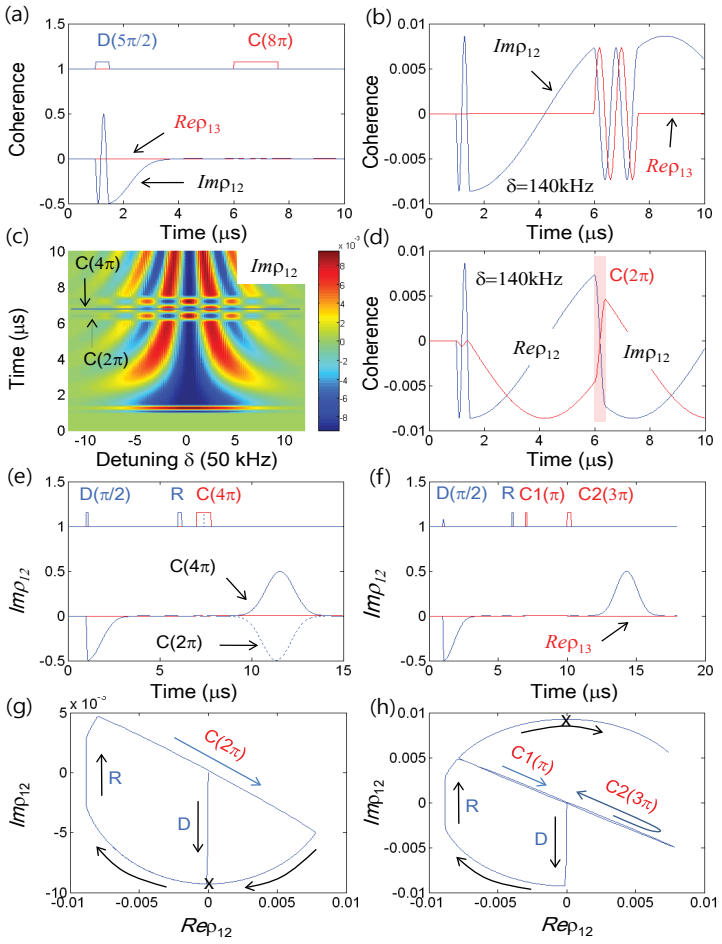

Figure 4: Atom phase control in a delayed Raman system. (a) Time-delayed light-matter interactions for the resonant Raman scheme of Figure 3. The pulse area of D and C is 5π/2 and 8π, respectively. (b) Coherence evolution of a detuned atom in (a). (c) A 3D color map of (a). (d) Coherence inversion by a 2π control pulse C in (b). (e) Atom phase control by C. (f) Controlled photon echo with C1(π) and C2(3π). (g) and (h) Bloch vector models for a detuned atom (δ=40 kHz) of (e) and (f), respectively. The mark 'x' is for the echo timing. Optical inhomogeneous broadening is 510 kHz (FWHM). All $\rho_{ij}(t=0)=0$, except for $\rho_{11}(t=0)=1$. All decay rates are zero. For calculations, a total 99.55% of the optical inhomogeneous width is divided into 121 groups at 10 kHz spacing

$$e^{\pm i\delta_j t} \overset{R(\pi)}{\rightarrow} e^{\mp i\delta_j T} e^{\pm i\delta_j t'} \left(= e^{\pm i\delta_j (t'-T)}\right) \tag{8}$$

Where $t' = t - t_R$. Thus, the first echo e1 is generated at $t = t_{e1} = t_R + T = 2T$ under population inversion. The echo e1 is supposed to be erased so as to not affect the second echo e2 via phase mismatch [31] or controlled phase turbulence [30,32,33,50-54].

The second π optical pulse RR (e-f) in Figures 5c and 5d arrives after e1 at $t = t_{e1} = t_R + T = 2T$ (or $t'' = t - (2T + T')$), rephases the system coherence again for the first echo e1 and each atom phase evolution continues in the time domain t'' (see the interval after f):

$$e^{\pm i\delta_j (t'-T)} \overset{RR(\pi)}{\rightarrow} e^{\mp i\delta_j (T+T'-T)} e^{\pm i\delta_j t''} \left(= e^{\pm i\delta_j (t''-T')}\right) \tag{9}$$

Where $t'' = t - (2T + T')$.

Thus, the second echo e2 is generated at $t = t_{e2} = 2(T + T')$ (see the mark 'x') with no population inversion (see the dotted curve in Figure 5b). This final echo e2, however, cannot be extracted from the medium because its macroscopic coherence is absorptive like the data pulse D. For better visualization, the experimental decay parameter γ is included, where the magnitude of e2 at point 'x' is smaller than the data excited coherence at point 'b.' This absorptive echo e2 is obvious, where double rephasing results in a 2π phase shift (i.e., no phase shift): $\rho(t) \overset{R1}{\rightarrow} \rho(t')^* \overset{R2}{\rightarrow} \rho(t'')$. Like the controlled AFC [25] discussed in Figure 4, the DR echoes [31-33] are also absorptive and thus impractical [29]. The observations of the DR echoes [31-33] are also due to the non-uniform pulse area applied to each atom, resulting from the Gaussian light distributed in the transverse spatial mode perpendicular (x- and y-axis) to the beam propagation direction (z-axis) [34]. To fix the absorptive echo e2 in Figure 5b, CDR echoes are introduced in Section E (Figure 5).

dc Stark echoes in a double rephasing scheme: An absorptive echo problem

The dc or ac Stark echo represents a technique for erasing the first echo e1 in DR echoes by using dc or ac Stark-induced phase turbulence, respectively [30,54]. The dc Stark control in the DR scheme of Figure 5 has the advantage of mitigating drawbacks of the gradient echoes [33], in which a persistent spectral holeburning, ultradense and bandwidth-limited optical medium is no longer a prerequisite. The ac Stark echo [30] is much simpler in configuration and has more advantages compared with its dc counterpart, where the dc Stark effect was first observed in two-pulse spin echoes half a century ago [50]. Here, the spin echoes are the magnetic version of photon echoes [60]. In both cases, two unbalanced Stark pulses are inserted across the first rephasing pulse R1, followed by the second rephasing pulse R2. Here "unbalanced" stands for the silencing condition of

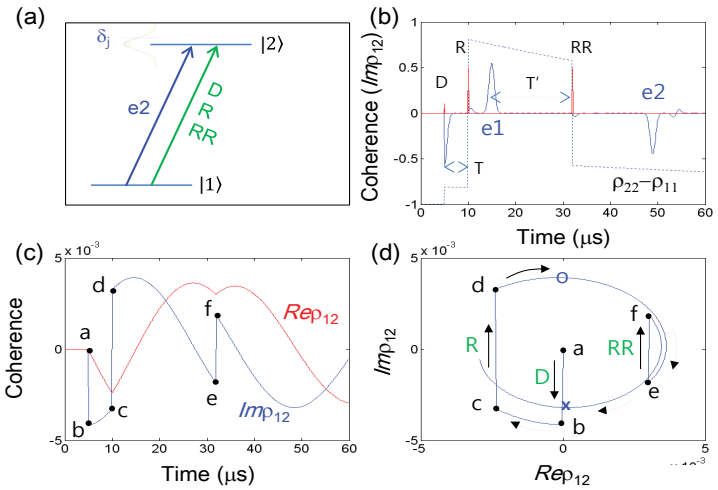

Figure 5: Double rephasing (DR) photon echoes. (a) A schematic of DR echoes. The pulse sequence is D(π/2), R(π) and RR(π). (b) Numerical simulations of DR echo: t_D=5; t_R=10; t_{RR}=32; t_{e1}=2t_R-t_D=15; t_{e2}=2t_{RR}-t_{e1}=2t_{RR}-2t_R+t_D=49 μs. (c) A detuned atom phase evolution at δ_j=20 kHz. (d) A Bloch vector model for (c). The mark 'o' ('x') indicates the timing of echo e1 (e2) in (b). The marks a-b, c-d, and e-f represent for D, R, and RR, respectively. The optical in homogeneous broadening is 680 kHz (FWHM); Γ_{21}=γ_{21}=1 kHz; ρ_{11}(t=0)=1. Each pulse duration is 0.1 μs. For calculations, a total 99.55% of the optical inhomogeneous width is divided into 161 groups at 10 kHz spacing

the first echo e1, where the second Stark pulse must come after e1 (Figure S4) [30,33]. In the dc Stark case, due to the ± Δω Stark splitting symmetry, the excited atoms (spins) by D are divided into two groups, resulting in fast and slow phase evolutions [61]. Thus, the phase accumulations between the two groups interfere with each other and cancel out under the specific condition of no echo generation [32,50,61]

$\rho_{12}=\sum\rho_{12}^{(j)}(e^{+i\Delta\omega\tau}+e^{-i\Delta\omega\tau})\alpha cos(\Delta\omega\tau)$. The silent echo condition for the first dc Stark shift is $\Phi_{DC1}=\Delta\omega\tau=(2n-1)\pi/2$. Interestingly, this silencing echo condition is exactly the same as in the ac Stark case, but in a different mechanism [30].

Because the second dc Stark shift must be the same as the first, their gradient polarity also must be same each other, and thus, it does not affect the phase on the second echo e2. This means that the second echo e2 has the same coherence as the D excited ensemble coherence: absorptive echo. The analytic solution for the dc Stark echoes is:

$$e^{\pm i\delta_j t}\xrightarrow{DC1}e^{\pm i\delta_j t}\left(e^{-i\Delta\omega_1\tau_1}+e^{+i\Delta\omega_1\tau_1}\right)\xrightarrow{R1}e^{\pm i\delta_j (t'-T)}\left(e^{+i\Delta\omega_1\tau_1}+e^{-i\Delta\omega_1\tau_1}\right)$$
$$\xrightarrow{DC2}\left(e^{+i\Delta\omega_1\tau_1}+e^{-i\Delta\omega_1\tau_1}+e^{+i\Delta\omega_2\tau_2}+e^{-i\Delta\omega_2\tau_2}\right).e^{\pm i\delta_j (t'-T)}\xrightarrow{R2}e^{\pm i\delta_j (t''-T')} \quad (10)$$

Where, $t'=t-T$, $t''=t-t_{R2}=t-(2T+T')$ and $\Phi_{DC1}=\Phi_{DC2}=\frac{\pi}{2}$. This result in equation (10) is the same as the doubly rephased echo e2 in equation (9) (see also the mark 'x' in Figure 5d for numerical calculations), whose coherence is absorptive, too.

Here, the detuning signs applied to the atoms by the dc (ac) Stark splitting are predetermined for each atom in a solid, i.e., the Stark fields are applied to the same atom groups without intermixing in rare-earth doped solids [62].

Controlled double rephasing (CDR) echoes

To solve the three major constraints of population inversion, ultralow retrieval efficiency and short storage time in conventional photon echoes, the CDR echo protocol has been proposed for quantum memory applications [29]. However, the main purpose of the CDR echo is to solve the absorptive echo problem in DR echoes, as seen in Figure 5. The solution model to overcome the ultralow retrieval efficiency and short storage time is given by Kerr ($\chi^{(3)}$) nonlinear optics induced by the control Rabi pulses in DR echoes [29]. Figure 6 represents the CDR echoes with the control pulse pair C1 and C2 added to the DR echo scheme, where quantum coherence control for the ensemble phase plays a key role in solving the absorptive photon echo dilemma in various modified photon echo schemes [25,31-33]. Unlike the π–3π control pulse sequence in a single rephasing scheme (Figure 4f) [57], a π–π control pulse sequence is required for the double rephasing scheme for emissive echoes (e2 in Figure 6b).

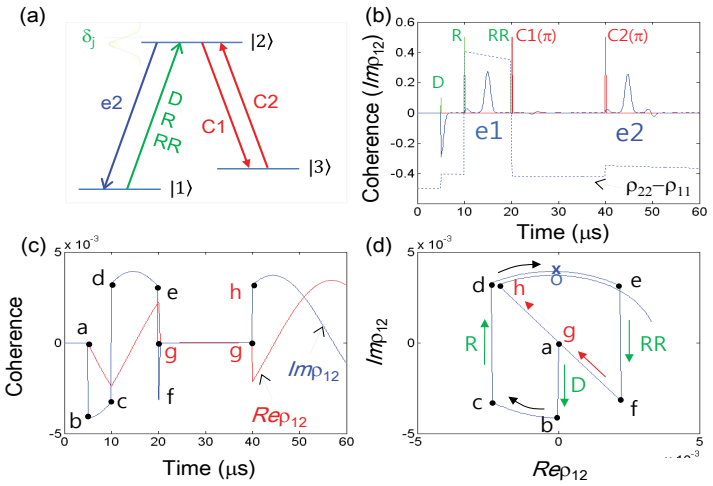

Figure 6: Controlled double rephasing (CDR) echoes. (a) A schematic of CDR echoes, where the control pulses C1 & C2 are added to a DD echo scheme in Figure 5. Pulses D, R, RR, C1, and C2 arrive at t=5, 10, 20, 20.1 and 40 μs. Each pulse duration is 0.1 μs. (b) Numerical calculations of the CDR echo in (a). Each pulse area is π, except for D (0.2π). (c) and (d) A detuned atom phase evolution for δ_j=20 kHz. The marks a-b, c-d, e-f, f-g, and g-h represent for D, R, RR, C1 and C2, respectively. The mark 'o' ('x') indicates echo e1 (e2). The optical inhomogeneous broadening is 680 kHz (FWHM); $\Gamma_{21}=\Gamma_{23}$=1 kHz; $\gamma_{21}=\gamma_{23}$=5 kHz 1 kHz; $\Gamma_{32}=\gamma_{32}$=0; ρ_{11}=1. The control pulse arrival time is t_{C1}=20.1 μs and t_{C2}=40 μs. The echo timing is $t_{e2}=2t_{RR}-t_{e1}+(t_{C2}-t_{C1})$=44.9 μs

Table 1: Photon echo-based quantum memory protocols

Quantum Memory protocol	Mechanism	Storage time	Retrieval efficiency (%)	Advantages	Disadvantages	Ref
CRIB (2001)	-Doppler shift -CCC	Spin T_2	~100	No rephasing pulse	Atomic diffusion (atomic vapors) (solids: rf rephasing)	[16] [17]
Gradient (2008)	-Spectral tailoring -Two levels -Three levels (Raman)	Optical T_2 Spin T_2 (Raman)	<100 <100 (Raman)	No rephasing pulse	-Atomic diffusion -Short storage time (10 ns~μs) -Spectral tailoring	[18,19] [20,21]
AFC (2008)	-Population grating -Accumulated coherence -Two levels	Optical T_2	<50 For multiple storage: ~1	No rephasing pulse	-Preparation time (~ms) -Short storage time	[22-24,26]
Controlled AFC (2010)	-Population grating -Accumulated coherence -CCC	Spin T_2	<50 -For mutimode: ~1	No rephasing pulse	-Preparation time (~ms)	[25]
†Optical locking (2009)	-Raman echo -CCC -Four levels	Spin T_1	<100	Ultralong storage	-Rephasing pulses -Population inversion	[27]
CDR (2-pulse) (2011)	-Two pulse echo -CCC -NDFWM	Spin T_2	~100	Ultralong storage	Rephasing pulses	[29]
CDR (3-pulse) (2012)	-Three pulse echo -CCC -NDFWM	Spin T_1	~100	Ultralong storage	Rephasing pulses	[28]
CASE (2017)	-Two pulse echo -NDFWM	Spin T_2	~100	Ultralong storage	Rephasing pulses	[30]

*CRIB: Controlled Reversible Inhomogeneous Broadening
*CCC: Controlled Coherence Conversion (Controlled Rabi flopping)
*CDR: Controlled Double Rephasing
*AFC: Atomic Frequency Comb
*CASE: Controlled ac Stark echoes
*Operating temperature: ~4K if the medium is a rare-earth doped solid
* In rare-earth doped solids, optical (Spin) T_2<ms. With Zeeman (or DD coupling), spin T_2~spin T_1 (s~min)
* In atomic vapors (e.g. Rb), optical (Spin) T_2~10 ns (~μs). With paraffin coating, spin T_2>ms
* Raman (Controlled) Gradient does not work in rare-earth doped solids due to spin inhomogeneity [20,21]
*All are multimode in time domain
†The original Optical locking protocol needs to be modified by adapting 3-pulse CDR (discussed elsewhere)

As shown in Figures 6c and 6d, an individual atom's coherence of the DR echo e2 at point 'f' experiences a complete coherence inversion by the control Rabi pulse pair. Thus, the system coherence reaches point 'h' through the point 'g,' where the point 'g' represents zero optical coherence: $e^{\mp i\delta T'} \rightarrow -e^{\mp i\delta T'}$; $T' = t_{RR} - t_{e1}$ (Equation (9)). Here, the optical coherence at 'g' is completely transferred to the spin state by C1: $\rho_{12} \rightarrow \rho_{13}$. The coherence evolution after C2 is denoted by $-e^{\pm i\delta(t''-T')}$,

Where,

$t'' = t - \left(2T + T' + T_C\right)$, $T = t_R - t_D$ and $T_C = t_{C2} - t_{C1}$

This means that the coherence $\rho_{12}(t)$ of echo e2 becomes emissive without population inversion at $t = 2\left(T + T'\right) + T_C$ (mark 'x' in Figure 6d).

It should also be noted that the zero optical coherence at point 'g' offers a storage time extension by T_C, which is determined by the spin phase decay time [16,17,25,29,48,55,56]. The storage time extension up to spin population decay time T_1 can be obtained via zero first-order Zeeman effects [43,63] or dynamic decoupling [44] through freezing the thermal spin bath. Even without magnetic fields or consecutive rf pulses for dynamic decoupling, the spin T_1-limited storage time can also be obtained by an optical locking technique [27,28], where the three-pulse photon echo scheme is required for the DR echo scheme. The control pulse set of C1 and C2 can also be positioned immediately after R but before e1 [58]. For the near unity echo retrieval efficiency, the counter-propagating C1 (π) and C2 (π) are used for the backward echo $e2\left(\boldsymbol{k}_{e2} = -\boldsymbol{k}_D + \boldsymbol{k}_{C1} + \boldsymbol{k}_{C2}\right)$ [16,56]. The echo efficiency based on this Kerr type nonlinearity depends on the spin coherence ρ_{13}, which is relied upon by the population transfer via the control Rabi pulses. Here, the rephasing pulses R and RR have nothing to do with the four-wave mixing processes for $\boldsymbol{k}_{e2}$ as experimentally demonstrated [56]. Thus, the backward echo in the CDR scheme has angle flexibility applicable to spatial multiplexing in a quantum interface, which is a great benefit in quantum network in the future.

CONCLUSION

Various modified photon echo protocols demonstrated for quantum memory applications were reviewed, analyzed, and discussed to give a clear understanding of collective atom phase control in controlled double rephasing (CDR) echoes. The ensemble phase control via control Rabi flopping between the excited state and an auxiliary third state was analyzed and discussed for the coherence inversion of a photon echo system in order to solve the problem of absorptive echoes in the double rephasing photon echo protocol. Several modified photon echo protocols such as controlled reversible inhomogeneous broadening, atomic frequency comb echoes, and dc/ac Stark echoes were reviewed to demonstrate the fundamental mechanisms (Table 1). Some critical misunderstandings such as absorptive coherence on the echo were discussed. The experimental echo observations in these wrong schemes are, however, due to both the Gaussian shape of control or rephrasing pulses in a transverse spatial mode as well as Beer's law-dependent absorption strength in the axial mode. To solve the inherent absorptive echo problem in the double rephasing scheme, a Rabi pulse set was added for collective atom phase control of the ensemble solid via Raman coherence transfer. As a result, the CDR echo protocol gives near perfect, inversion-free, emissive, and storage time-extended photon echoes for quantum memory applications. Moreover, the backward CDR echo scheme offers a great benefit of spatial multiplexing for multimode spatial quantum interfaces in the future quantum networks. To avoid coherence leakage in an actual apparatus, firstly, the spatial transverse mode of the optical control pulses should be made uniform, and secondly, the Beer's law-dependent absorption strength should be flattened (will be discussed elsewhere). Eventually CDR echoes will pave the road to not only quantum memories applicable to quantum repeaters for long distance quantum communications, but also to scalable qubits for fault-tolerant quantum computing, where the storage time can be extended up to the spin population decay time in the order of minutes in a rare-earth Pr^{3+} doped YSO crystal

ACKNOWLEDGEMENT

This work was supported by the ICT R&D program of MSIT/IITP (1711042435: Reliable crypto-system standards and core technology development for secure quantum key distribution network).

REFERENCES

[1] Gisin ON, Ribordy G, Tittel W, Zbinden H, Quantum cryptography. *Rev Mod Phys*, **2002**, 74: 145.

[2] Jouguet P, Kunz-Jacques S, Leverrier A, Grangier P, Diamanti E. Experimental demonstration of long-distance continuous-variable quantum key distribution. *Nature Photon*, **2013**, 7: 378.

[3] Curty M, Xu F, Cui W, Lim K, Tamaki, et al. Finite key analysis for measurement-device-independent quantum key distribution. *Nature Commun*, **2014**, 5: 3732.

[4] Hensen B. Loophole-free Bell inequality violation using electron spins separated by 1.3 km. *Nature*, **2015**, 526: 682.

[5] Ladd TD, Jelezko F, Laflamme R, Nakamura Y, Monroe C, et al. Quantum computers. *Nature*, **2010**, 464: 45.

[6] Martinis JM. Qubit metrology for building a fault-tolerant quantum computer. *NPJ Quant Inf*, **2015**, 1: 15005.

[7] Nigg D, Müller M, Martinez EA, Schindler P, Hennrich M, et al. Quantum computations on a topologically encoded qubit. *Science*, **2014**, 345: 302.

[8] Bernien H. Probing many-body dynamics on a 1-atom quantum simulator. *arXiv*, **2017**, 17: 579-584.

[9] Mons T. 14-Qubit entanglement: Creation and coherence. *Phys Rev Lett*, **2011**, 106: 130506.

[10] Duan LM, Lukin MD, Cirac JI, Zoller P. Long-distance quantum communications with atomic ensembles and linear optics. *Nature*, **2001**, 414: 413.

[11] Sangouard N, Simon S, de Riedmatten H, Gisin N. Quantum repeaters based on atomic ensembles and linear optics. *Rev Mod Phys*, **2011**, 83: 33.

[12] O'Brien JL. Optical quantum computing. *Science*, **2007**, 318: 1567.

[13] Briegel HJ, Browne DE, Dür W, Raussendorf R, Van den Nest M. Measurement based quantum computation. *Nature Phys*, **2009**, 5: 19.

[14] Choi KS, Deng H, Kimble HJ. Mapping photonic entanglement into and out of a quantum memory. *Nature*, **2008**, 452: 67.

[15] Kurnit NA, Abella ID, Hartmann SR. Observation of a photon echo. *Phys Rev Lett*, **1964**, 13: 567.

[16] Moiseev SA, Kröll S. Complete reconstruction of the quantum state of a single-photon wave packet absorbed by a Doppler-broadened transition. *Phys Rev Lett*, **2001**, 87: 173601.

[17] Moiseev SA, Tarasov VF, Ham BS. Quantum memory photon echo-like techniques in solids. *J Opt B Quantum Semiclass Opt*, **2003**, 5: S497.

[18] Hetet G, Longdell JJ, Alexander AL, Lam PK, Sellars MJ. Electro-optic quantum memory for light using two-level atoms. *Phys Rev Lett*, **2008**, 100: 023601.

[19] Hedges MP, Longdell JJ, Li Y, Sellars MJ. Efficient quantum memory for light. *Nature*, **2010**, 465: 1052.

[20] Hosseini M, Sparkes BM, Hetet G, Longdell JJ, Lam PK, et al. Coherent optical pulse sequencer for quantum applications. *Nature*, **2009**, 461: 241.

[21] Hosseini M, Sparkes BM, Campbell G, Lam PK, Buchler BC. High efficiency coherent optical memory with warm rubidium vapour. *Nature Commun*, **2011**, 2: 174.

[22] de Riedmatten H, Afzelius M, Staudt MU, Simon C, Gisin N. A solid-state light-matter interface at the single-photon level. *Nature*, **2008**, 456: 773.

[23] Saglamyurek E, Sinclair N, Jin J, Slater JA, Oblak D, et al. Broadband waveguide quantum memory for entangled photons. *Nature*, **2011**, 469: 512.

[24] Usmani I, Afzelius M, de Riedmatten H, Gisin N, Mapping multiple photonic qubits into and out of one solid-state atomic ensemble. *Nature Commun*, **2010**, 1: 12.

[25] Afzelius M, Usmani I, Amari A, Lauritzen B, Walther A, et al. Demonstration of atomic frequency comb memory for light with spin-wave storage. *Phys Rev Lett*, **2010**, 104: 040503.

[26] Zhong T. Nanophotonic rare-earth quantum memory with optically controlled retrieval. *Science*, **2017**, 10: 1126.

[27] Ham BS. Ultra-long quantum optical data storage using an optical locking technique. *Nature Photon*, **2009**, 3: 518.

[28] Ham BS. Coherent control of collective atom phase for ultra-long, inversion-free photon echoes. *Phys Rev A*, **2012**, 85: 031402.

[29] Ham BS. Atom phase controlled noise-free photon echoes. *arXiv*, **2011**, 1: 5480.

[30] Ham BS. A controlled ac Stark echoes for quantum memories. *Sci Rep*, **2017**, 7: 7655.

[31] Damon V, Bonarota M, Louchet-Chauvet A, Chanelière T, Le Gouët JL. Revival of silenced echo and quantum memory for light. *New J Phys*, **2011**, 13: 093031.

[32] Arcangeli A, Ferrier A, Goldner PH. Stark echo modulation for quantum memories. *Phys Rev A*, **2016**, 93: 062303.

[33] McAuslan DL, Ledingham PM, Naylor WR, Beavan SE, Hedges MP, et al. Photon-echo quantum memories in an inhomogeneously broadened two-level atoms. *Phys Rev A*, **2011**, 84: 022309.

[34] Ham BS. Gaussian beam-caused imperfect rephasing in photon echo-based quantum memories. *arXiv*, **2017**, 1: 04291.

[35] Ham BS. Investigation of quantum coherence excitation and coherence transfer in an inhomogeneously broadened rare-earth doped solid. *Opt Exp*, **2008**, 16: 5350.

[36] Hau LV, Harris SE, Dutton Z, Behroozi H. Light speed reduction to 17 m/s in an ultracold atomic gas. *Nature*, **1999**, 397: 594.

[37] Philips DF, Fleischhauer A, Mair A, Walsworth RL, Lukin MD. Storage of light in atomic vapor. *Phys Rev Lett*, **2001**, 86:783.

[38] Turukhin AV, Sudarshanam VS, Shahriar MS, Musser JA, Ham BS, et al. Observation of ultraslow and stored light pulses in a solid. *Phys Rev Lett*, **2002**, 88: 023602.

[39] Sargent M, Scully MO, Lamb Jr WE. Valuable book on laser physics: Laser Physics. *Laser Phys*, **1974**.

[40] Ziolkowski RW, Arnold JM, Gogny DM. Ultrafast pulse interactions with two-level atoms. *Phys Rev A*, **1995**, 52: 3082.

[41] Macfarlane RM, Shelby RM. Coherent transient and hole burning spectroscopy of rare earth ions in solids. In: Spectroscopy of solids containing rare earth ions. Kaplyanskii A, Macfarlane RM (edtrs), North-Holland, **1987**.

[42] Mossberg TW. Time-domain frequency-selective optical data storage. *Opt Lett*, **1982**, 7: 77.

[43] Langer C. Long-lived qubit memory using atomic ions. *Phys Rev Lett*, **2005**, 95: 060502.

[44] Bar-Gill N, Pham LM, Jarmola A, Budker D, Walsworth RL. Solid-state electronics spin coherence time approaching one second. *Nature Commun*, **2013**, 4: 1743.

[45] Sangouard N, Simon C, Afzelius M, Gisin N. Analysis of a quantum memory for photons based on controlled reversible inhomogeneous broadening. *Phys Rev A*, **2007**, 75: 032327.

[46] Hemmer PR, Cheng KZ, Kierstead J, Shahriar MS, Kim MK. Time-domain optical data storage by use of Raman coherent population trapping. *Opt Lett*, **1994**, 19: 296.

[47] Ham BS, Shahriar MS, Kim MK, Hemmer PR. Spin coherence excitation and rephasing with optically shelved atoms. *Phys Rev B*, **1998**, 58: R11825.

[48] Ham BS. Analysis of optical locking applied for rephasing halt in photon echoes. *J Opt Soc Am B*, **2011**, 28: 775.

[49] Ham BS. A contradictory phenomenon of deshelving pulses in a dilute medium used for lengthened photon storage time. *Opt Exp*, **2010**, 18: 17749.

[50] Mims WB, Electric field effects in spin echoes. *Phys Rev*, **1964**, 133: A835.

[51] Meixner AJ, Jefferson CM, Macfarlane RM. Measurement of the Stark effect with sub-homogeneous line width resolution in Eu^{3+}:$YAlO_3$. *Phys Rev B*, **1992**, 46: 5912.

[52] Wang YP, Boye DM, Rives JE, Meltzer RS. Modulation of photon echo intensity by pulsed non-uniform magnetic fields. *J Lumin*, **1990**, 45: 437.

[53] Hétet G, Hosseini M, Sparkes BM, Oblak D, Lam PK, et al. Photon echoes generated by reversing magnetic field gradients in a rubidium vapor. *Opt Lett*, **2008**, 33: 2323.

[54] Chaneliere T, Hetet G. Light-shift-modulated photon-echo. *Opt Lett*, **2015**, 40: 1294.

[55] Ham BS, Hemmer PR, Shahriar MS. Efficient phase conjugation via two-photon coherence in an optically dense crystal. *Phys Rev A*, **1999**, 59: R2583.

[56] Hahn J, Ham BS. Rephasing halted photon echoes using controlled optical deshelving. *New J Phys*, **2011**, 13: 093011.

[57] Ham BS. Control of photon storage time using phase locking. *Opt Exp*, **2010**, 18: 1704.

[58] Rhamattullah, Ham BS. Analysis of controlled coherence conversion in a double rephasing scheme of photon echoes for quantum memories. *arXiv*, **2016**, 12: 02167.

[59] Rhamattullah, Ham BS. Understanding of collective atom phase control in modified photo echoes for a near perfect, storage time extended quantum memory. *arXiv*, **2017**, 3: 03668.

[60] Hahn EL. Spin echoes. *Phys Rev*, **1950**, 80: 580.

[61] Ellitt RJ. Crystal field theory in the rare earths. *Rev Mod Phys*, **1953**, 25: 167.

[62] Ludwig GW, Woodbury HH. Splitting of electron spin resonance lines by an applied electric field. *Phys Rev Lett*, **1961**, 7: 240.

[63] Zhong M, Hedges MP, Ahlefeldt RL, Bartholomew JG, Beavan SE, et al. Optically addressable nuclear spins in a solid with a 6 h coherence time. *Nature*, **2015**, 517: 177-181.